

1 **Interactions between increasing CO₂ and Antarctic melt rates**

2 Shona Mackie*

3 *Department of Physics, University of Otago, Dunedin, New Zealand*

4 Inga J. Smith

5 *Department of Physics, University of Otago, Dunedin, New Zealand*

6 David P. Stevens

7 *School of Mathematics, University of East Anglia, Norwich, U.K.*

8 Jeff K. Ridley

9 *Met Office, Exeter, U.K.*

10 Patricia J. Langhorne

11 *Department of Physics, University of Otago, Dunedin, New Zealand*

12 *Corresponding author address: Department of Physics, University of Otago, Dunedin 9016, New
13 Zealand

14 E-mail: shona.mackie@otago.ac.nz

ABSTRACT

15 Meltwater from the Antarctic ice sheet is expected to increase the sea ice
16 extent. However, such an expansion may be moderated by sea ice decline
17 associated with global warming. Here we investigate the relative balance of
18 these two processes through experiments using HadGEM3-GC3.1, and com-
19 pare these to two standard idealised CMIP6 experiments. Our results show
20 that the decline in sea ice projected under scenarios of increasing CO₂ may
21 be inhibited by simultaneously increasing melt fluxes. We find that Antarc-
22 tic Bottom Water formation, projected to decline as CO₂ increases, is likely
23 to decline further with an increasing meltwater flux. In our simulations, the
24 response of the westerly wind jet to increasing CO₂ is enhanced when the
25 meltwater flux increases, resulting in a stronger peak wind stress than is found
26 when either CO₂ or melt rates increase exclusively. We find that the sensitivity
27 of the Antarctic Circumpolar Current to increasing melt fluxes in the South-
28 ern Ocean is countered by increasing CO₂, removing or reducing a feedback
29 mechanism that may otherwise allow more heat to be transported to the polar
30 regions and drive increasing ice shelf melt rates. The insights presented here,
31 and in the accompanying paper (which focuses on the effect of increasing melt
32 fluxes under pre-industrial forcings) provide insights helpful to the interpre-
33 tation of both future climate projections and sensitivity studies into the effect
34 of increasing melt fluxes from the Antarctic ice sheet when different forcing
35 scenarios are used.

36 **1. Introduction**

37 Meteoric ice from Antarctica flows through the grounding line of the ice shelves and either
38 melts from the ice shelf bases into the ocean, or calves from the ice shelf fronts as icebergs that are
39 transported and melt. Sublimation and surface runoff are small compared to the rates of mass loss
40 through icebergs and ice shelf melt in the Antarctic (Liston and Winther 2005). The meltwater that
41 enters the ocean is fresh and therefore buoyant, and so it can drive a stratification that inhibits mix-
42 ing and prevents warm deeper waters from influencing the surface, promoting sea ice production
43 and inhibiting sea ice basal melt (Bintanja et al. 2015; Mackie et al. submitted). This contrasts with
44 the effect of increasing CO₂, which has a warming effect that inhibits sea ice production. Sea ice
45 is more reflective than the ocean surface, and so changes in sea ice cover represent changes to the
46 planetary albedo and affect the Earth's radiation budget through the temperature-albedo feedback
47 (Rind et al. 1995), with potential implications for almost all aspects of climate. Furthermore, by
48 creating a physical barrier between the ocean and atmosphere, sea ice alters the amount of precip-
49 itation reaching the ocean. This has implications for local ocean salinity, which is further affected
50 by brine rejection associated with sea ice production, and surface freshening associated with sea
51 ice melt (Weeks 2010). Changes to ocean salinity from these processes can impact ocean density
52 differences that drive much ocean circulation (Bromwich et al. 1998). The insulating effect of sea
53 ice can also result in a locally warmer ocean and cooler atmosphere as less heat is transferred from
54 the former to the latter (Andreas and Murphy 1986; Bromwich et al. 1998; Bronselaer et al. 2018;
55 Mackie et al. submitted). Changes to sea ice cover, driven by the competing effects of increasing
56 CO₂ and increasing melt fluxes from Antarctica, can therefore result in ocean and climate changes
57 that extend beyond the sea ice edge, requiring appropriate representation in climate models.

58 Increases in CO₂ are generally included in calculations of the likely future climate, however
59 increases in the rate at which meteoric ice is lost from Antarctica are generally not considered (i.e.
60 the rate is assumed constant), or are underestimated compared to glaciological estimates. This
61 study builds on a parallel study, which looked at the effect of increasing melt rates, and considers
62 where the effect of an increasing meltwater flux may enhance or reduce some climate effects
63 attributable to increasing levels of CO₂.

64 An increase in meteoric ice melt fluxes entering the Southern Ocean results in a cooling of the
65 ocean surface, increased sea ice cover and a colder lower atmosphere. Such a shift in the thermo-
66 dynamics results in a northwards shift of the meteorological polar front, the boundary between the
67 air masses of the polar cell and the Ferrell cell, and of the intertropical convergence zone (ITCZ)
68 (Bronselaeer et al. 2018; Mackie et al. submitted). An increase in meltwater causes a surface fresh-
69 ening, potentially reducing the meridional density gradient (Mackie et al. submitted), which is a
70 driver for the Antarctic Circumpolar Current (ACC) (Russell et al. 2006). The ACC is related to
71 the amount of heat transported from the low to high latitude ocean, and changes in its strength may
72 therefore affect ice shelf melt by influencing the heat that reaches the ice shelf fronts. Stratification
73 can inhibit deeper waters from rising to the surface to exchange heat and gas with the atmosphere.
74 Via this mechanism, an increase in melt fluxes can cause mid-layer ocean waters to warm (Bron-
75 selaeer et al. 2018; Mackie et al. submitted). If the meltwater enters at depth along the ice shelf
76 fronts, then it can become supercooled as it rises to the surface, forming frazil ice crystals in the
77 water column that rise to the surface to form new sea ice, or attach to the underside of existing sea
78 ice, enhancing sea ice growth (Weeks 2010; Mackie et al. submitted). If the volume of the melt
79 entering the ocean at depth is high enough, then this rising water can drive a local overturning
80 (Merino et al. 2018), and a freshening of the whole water column that inhibits the formation of
81 Antarctic Bottom Water (AABW) (Mackie et al. submitted). AABW is usually formed as dense

82 saline water, created by brine rejection during sea ice production at some key locations, sinks
83 from the surface to the continental shelf, from where it spills over to fill the deep ocean basins.
84 AABW formation constitutes the southern end of the thermohaline circulation, which is an impor-
85 tant mechanism by which heat is distributed around the planet (Weaver et al. 2003; Sloyan 2006;
86 Marsland et al. 2007). As the upper ocean warms and its density decreases with increasing levels
87 of CO₂, AABW formation is anticipated to reduce, and this reduction could be enhanced by the
88 decrease in AABW that is driven by the simultaneously increasing melt fluxes. It is important that
89 any change to AABW formation is represented realistically in climate models in order for reliable
90 projections to be made of high southern latitude ocean properties and circulation.

91 Previous works have found the position and strength of the westerly winds around Antarctica,
92 driven by the latitudinal temperature gradient in combination with the planetary rotation, to be im-
93 pacted by Antarctic sea ice extent (Kidston et al. 2011; Mackie et al. submitted). The circumpolar
94 winds are associated with mid-latitude weather in the Southern Hemisphere (Hoskins and Hodges
95 2005; Le Quéré et al. 2007), and are anticipated to strengthen and to shift to higher latitudes under
96 future climate warming (Bracegirdle et al. 2013). This raises the question of whether their sen-
97 sitivity to sea ice extent could be enhanced in a warming climate. We consider whether sea ice
98 changes, driven by increasing melt fluxes, could offset or compound the changes to the westerlies
99 that are attributable to rising temperatures.

100 The latest generation of the HadGEM model, HadGEM3-GC3.1 includes several improvements
101 to the representation of sea ice and ocean processes (Ridley et al. 2018; Storkey et al. 2018), includ-
102 ing a realistic spatial distribution of ice shelf melt from Rignot et al. (2013), a new parametrization
103 for ice shelf basal melt (Mathiot et al. 2017), and explicit representation of icebergs (Marsh et al.
104 2015). However, in common with most climate models, the rate of mass loss from the Antarctic
105 continent remains constant, and climate projections submitted to the CMIP6 experiment are cal-

106 culated on this basis. In reality, the rate of mass loss is known to be increasing for at least some
107 ice shelves (Rignot et al. 2008; Sutterley et al. 2014; Martin-Espanol et al. 2016; Shepherd et al.
108 2018), and it is likely that further increases will occur as the climate warms in future (Timmer-
109 mann and Hellmer 2013). Studies into the sensitivity of climate models to this assumption have
110 shown that impacts on sea ice and ocean processes are likely, but different results have been found
111 in different works, for example Richardson et al. (2005); Turner et al. (2013); Bintanja et al. (2013,
112 2015); Zunz and Goosse (2015); Swart and Fyfe (2013); Pauling et al. (2016, 2017); Merino et al.
113 (2018); Bronselaer et al. (2018). The modelling advances included in HadGEM3-GC3.1 make it
114 appropriate to revisit this question and investigate the impact of increasing rates of Antarctic mass
115 loss for climate projections made using this model.

116 Reliable projections of global climate require sea ice and ocean processes to be appropriately
117 represented in climate models, and so it is important to consider the impact that increasing Antarc-
118 tic melt rates may have on these, and whether these could enhance or inhibit effects attributable to
119 CO₂-induced warming. We investigate the behaviour of these characteristics in the CMIP6 model
120 HadGEM3-GC3.1. In the accompanying paper, the effects of increasing rates of iceberg and ice
121 shelf melt are reported assuming external greenhouse gas forcings to be fixed at pre-industrial
122 levels (Mackie et al. submitted). Here, we evaluate whether these same sensitivities occur in an
123 environment where CO₂ increases simultaneously with the melt rate (both are applied as external
124 forcings), and assess whether the sensitivity of some ocean and sea ice processes to an increasing
125 melt rate could enhance, or partially counter, the effects of CO₂-induced warming.

126 **2. Method**

127 *Model Description*

128 HadGEM3-GC3.1 (Williams et al. 2017; Kuhlbrodt et al. 2018) is the coupled land-ocean-sea
129 ice-atmosphere model that forms the physical core of the UK Earth System Model, and is the basis
130 from which the New Zealand Earth System Model is being developed (Williams et al. 2016). It
131 uses GA7-GL7 for the atmosphere and land (Walters et al. 2019), GO6 for the ocean (Storkey
132 et al. 2018), and GSI8.1 for the sea ice component (Ridley et al. 2018). For this work, we use
133 the ORCA1 grid (nominally 1° resolution) for the ocean and sea ice, and a resolution of 1.875°
134 by 1.25° for the atmosphere. The ocean is configured with 75 vertical layers, and the atmosphere
135 with 85. Mass loss from Antarctica in the standard configuration of the model is kept constant
136 at a rate of 1770.75 Gt / year (set so as to maintain the ice sheets in mass balance under pre-
137 industrial forcings). Excepting a small amount of accumulation that melts or sublimates at the
138 surface (according to atmospheric conditions over Antarctica), the mass loss is distributed around
139 the coastal ice shelves following the distribution in Rignot et al. (2013). 45% of the mass flux
140 at each ice shelf constitutes an iceberg calving flux, wherein icebergs are created following the
141 size distribution from Bigg et al. (1997). Icebergs travel and melt according to ocean surface
142 properties, following the Lagrangian scheme in Mathiot et al. (2017), with a cooling effect on the
143 surface ocean from the melt due to the latent heat. The remaining 55% of the mass flux represents
144 ice shelf basal melt, which is distributed vertically between the average grounding line depth and
145 the base of the ice shelf at its front, according to the parametrization in Mathiot et al. (2017) (the
146 cavity is not explicitly represented). The rate of mass loss from the Greenland Ice Sheet is also
147 assumed constant, and similar processes are followed, but with a calving rate of 100% since there
148 are assumed to be no ice shelves.

149 *Experiments*

150 Two standard HadGEM3-GC3.1 CMIP6 simulations, the pre-industrial control (PIControl) and
151 the 1% per annum increasing CO₂ (CO2), provide the reference experiments for this study. Note
152 that in the CMIP6 1% CO₂ simulation, CO₂ reaches four times pre-industrial levels after 140
153 years, but CO2 comprises only the first 100 years of this simulation. We undertake additional
154 simulations, intended to assess the effect of an increasing rate of mass loss from Antarctica relative
155 to PIconrol (mass loss from the Greenland Ice Sheet remains as per the standard model in all
156 experiments). The first experiment, FW, investigates the sensitivity of the modelled ocean and sea
157 ice to an increasing rate of total mass loss from the Antarctic continent, and is discussed by Mackie
158 et al. (submitted). All external forcings in FW (except Antarctic mass loss) are held constant at
159 pre-industrial levels. In the second experiment, FWCO2, CO₂ increases by 1% annually, as for
160 the reference simulation, CO2, and the same increase in Antarctic mass loss is applied as for FW
161 (both the mass loss and the CO₂ are prescribed as external forcings, and so are not coupled to
162 each other in FWCO2). All other external forcings are held constant. FWCO2 addresses two
163 questions: first, whether the sensitivities found in FW for a pre-industrial world also apply in
164 a world with increasing CO₂; and second, whether the effect of the additional meltwater could
165 counter, or enhance, effects attributable to increasing CO₂. In FW and FWCO2, the increased
166 mass loss is distributed spatially around the continent, and proportioned between ice shelf basal
167 melt and an iceberg calving flux, as for the standard model. The total rate of mass loss in FW and
168 FWCO2 is increased by 2.33% each year for 100 years, so that the rate of mass loss after 100 years
169 is ten times the initial rate (Figure 1). The scenario was designed to look at the sensitivity of the
170 modelled ocean and sea ice to the increasing rate of mass loss, rather than to be realistic in terms
171 of absolute numbers. For context, the freshwater contribution from Antarctica to the Southern

172 Ocean could rise above 1 Sv (31104 Gt / year using HadGEM3-GC3.1's 360 day model year) by
173 the year 2100 under RCP 8.5 (DeConto and Pollard 2016), which is almost twice the maximum
174 reached in our experiments (17707.5 Gt / year). The configurations for the different simulations
175 are summarised in Table 1, and the data are publicly available at Mackie et al. (2020). Anomalies
176 presented later are the result of subtracting the value for a diagnostic in PICOntrol from the value
177 for the same diagnostic in the experiment for the equivalent model time.

178 *Spatial Distribution of the Additional Freshwater Forcing*

179 The mean spatial distribution of the melt flux in PICOntrol is shown in Figure 2a, alongside
180 the anomaly showing the effect of the warming ocean surface on the meltwater distribution for
181 the final 20 years of CO₂ (Figure 2b), and the anomalies showing how the additional melt flux is
182 distributed for the final 20 years of FW and FWCO₂ (Figure 2c and d). Ocean surface properties
183 in CO₂ and PICOntrol differ, affecting iceberg trajectories and lifetimes, although both simulations
184 are subject to the same total volume of iceberg mass. Similarly, the increased iceberg mass that
185 is calved from the ice shelves is the same in FW as in FWCO₂, but the additional iceberg melt is
186 distributed differently because the ocean surface is warmer in FWCO₂, and thus icebergs melt at
187 higher latitudes.

188 **3. Results**

189 *Sea Ice Effects*

190 Antarctic sea ice trends are spatially variable (Cavalieri and Parkinson 2008) and so we assess
191 the sea ice response separately for the different ocean sectors in Figure 3 (sectors defined following
192 Yuan et al. (2017)). The total melt flux entering each sector is shown in Figure 4, and in this section

193 we examine the sea ice response to this by looking at changes in sea ice area (SIA) (Figure 5) and
194 thickness (Figure 6), relative to PICOntrol for the final 30 years of the simulations.

195 In CO₂, sea ice area (Figure 5a) and thickness (Figure 6b) reduce as CO₂ increases and tem-
196 peratures rise, however this decrease is smaller than the increases in SIA and sea ice thickness
197 attributable to increasing melt fluxes in FW (Figure 5a and Figure 6c). The combined effect of in-
198 creasing melt fluxes and CO₂ in FWCO₂ is a similar total SIA for the whole southern hemisphere
199 to PICOntrol (Figure 5a), rather than a net increase, because the warming ocean confines sea ice
200 production to higher latitudes. This means that a greater proportion of the additional meltwater in
201 FWCO₂ enters the ocean where sea ice is unlikely to form, making the sensitivity of sea ice to the
202 additional melt fluxes in FWCO₂ less pronounced than in FW. Higher ocean temperatures in CO₂
203 mean that where sea ice does form, it is thinner than in PICOntrol (Figure 6b). In FWCO₂, the ad-
204 ditional melt fluxes mean that this lack of growth is partially offset, and in some places overcome,
205 to result in thicker sea ice than in PICOntrol (Figure 6d).

206 Regionally, the competing effects of the simultaneously increasing melt flux and CO₂ in the
207 Ross Sea and Indian Ocean result in no net change to SIA in FWCO₂, relative to PICOntrol (Fig-
208 ure 5b, e). The Amundsen-Bellinghausen and Weddell Sea sectors receive the largest additional
209 melt flux (Figure 4c, d), and so melt-induced SIA-enhancing effects may be anticipated to be
210 stronger here than in the other sectors, and therefore more likely to override the effects of the CO₂.
211 In both sectors, however, some ice shelf basal meltwater and icebergs are likely to be transported
212 by the coastal current and the gyres (Figure 3b). The Ross Gyre and coastal current carry some
213 meltwater from the Amundsen-Bellinghausen Sea into the Ross Sea (freshwater transport across
214 the boundary between these two sectors is plotted in Figure S1 in the online supplemental mate-
215 rial), and the Weddell Gyre carries icebergs, and some meltwater, generated in the Weddell Sea,
216 northwards to latitudes where sea ice is unlikely to form (Figure 2). This means that the increasing

217 meltwater does not fully offset the SIA reduction driven by the CO₂, and SIA may in fact decrease
218 slightly over the latter part of FWCO₂ in these sectors (Figure 5c, d). The decrease is small, and
219 its persistence over a longer experiment would be required to determine whether effects from the
220 increasing CO₂ locally dominate over those from the increasing melt fluxes.

221 The inclusion of increasing ice shelf and iceberg melt fluxes in FWCO₂ serves to offset the
222 decline in sea ice concentration in all sectors, cancelling it altogether (relative to pre-industrial
223 conditions) in every sector except the Amundsen-Bellinghousen Sea, where the additional fresh-
224 water weakens the decline, but does not altogether remove it (Figure 5c). Data derived from
225 satellite observations show sea ice around Antarctica to have been advancing in most areas in re-
226 cent years, with the exception of the Amundsen-Bellinghousen Sea where the area has reduced,
227 while climate models generally calculate it to be in decline everywhere (Cavaliere and Parkinson
228 2008; Stammerjohn et al. 2008; Turner et al. 2009). These results show that simulations where
229 both CO₂ and meltwater fluxes increase simultaneously result in modeled sea ice area trends that
230 agree more closely with satellite-derived datasets. It should be noted, however, that these are ide-
231 alised simulations and realistic estimates for the increases in both CO₂ and meltwater depend on
232 the future scenario assumed for greenhouse gas emissions.

233 The downward salt flux model output can be used as a proxy for sea ice production and used to
234 identify areas of sea ice growth and decay. Before sea ice forms, all salt is in the ocean. When
235 sea ice forms in the model, despite some brine rejection, both salt and freshwater are removed
236 from the ocean and the salt is trapped in the sea ice (the salt amount is constant per unit volume of
237 sea ice). Hence there is less salt than before in the ocean, and this constitutes an upward salt flux
238 at the ocean surface. When sea ice melts, salt is returned to the ocean, constituting a downward
239 salt flux at the ocean surface. The total salt content of the ocean is otherwise conserved and is
240 unchanged by processes of adding fresh water or evaporation. Note that, since sea ice is relatively

241 fresh, less salt is removed during sea ice production than is contained in the volume of ocean water
242 that freezes, and the salinity of surface waters therefore increases with sea ice production.

243 Antarctic sea ice forms primarily in polynyas at the coast, although some also forms in the open
244 ocean from frazil crystals at the surface, which in windless conditions, form a continuous flexible
245 layer of thin ice, called nilas (as observed for example by Winsor and Björk (2000); Smedsrud
246 and Skogseth (2006)). In windy conditions, wave action drives the formation of pancake ice from
247 the frazil (Dai et al. 2004; Maksym 2012). The sea ice generally thickens through congelation
248 (downward growth of ice crystals into the ocean), and through the accumulation of snow on the
249 upper surface (Weeks 2010; Maksym 2012). Most Antarctic sea ice is transported equator-wards
250 and subsequently melts at the ice margins where the ocean is warmer (Weeks 2010; Maksym
251 2012).

252 Sea ice growth is greatest in June, July and August in all experiments (the seasonal cycle for
253 the simulations is plotted in the online supplemental material (Figure S2)). To assess changes
254 to the spatial distribution of sea ice production, the mean anomaly in the downward salt flux for
255 these months is shown in Figure 7 for the final 30 years of all experiments, alongside the mean
256 downward saltflux from PICOntrol for the same months. The positive (red) salt flux at the northern
257 edge of the plotted data for PICOntrol (Figure 7a) represents melting sea ice. In CO₂, this flux is
258 reduced since there is less sea ice here to melt in CO₂ (Figure 6b), creating the negative (blue)
259 anomaly at the northern edge of Figure 7b. Areas corresponding to a positive (red) anomaly in
260 CO₂ represent areas where sea ice production in PICOntrol is reduced, or has been replaced by sea
261 ice melt. There is a slight increase in sea ice production in the Weddell and Ross Seas in CO₂, and
262 close to the coast around the western Indian Ocean, indicated by the blue anomaly in Figure 7b.

263 The salt flux anomaly for CO₂ (Figure 7b) is spatially almost the inverse of that for FW (Figure
264 7c). In FW, the northern melt edge is further north than in PICOntrol because the sea ice has ex-

265 panded (Figure 6b). This creates the positive (red) anomaly at the northern edge in FW (since there
266 is no sea ice here to melt in PICOntrol). The ring-like negative (blue) anomaly in FW indicates
267 both reduced sea ice melt, and increased sea ice production (Figure 7c), relative to PICOntrol.
268 Southwards of this blue ring, there is a positive anomaly in FW, which is particularly strong in
269 the outer Weddell and Ross Seas, and in the western Indian Ocean. While sea ice production has
270 increased strongly further north in FW, it has decreased slightly here, relative to PICOntrol. In
271 the Western Pacific, where the continental shelf edge is close to the coast (Figure 3a), the posi-
272 tive (red) anomaly at the coast in FW shows a reduction in sea ice production, while the negative
273 (blue) anomaly beyond the coast, and beyond the continental shelf edge, shows increased sea ice
274 production (Figure 7c). This shift of at least some sea ice production in this area to beyond the
275 continental shelf edge in FW is also seen, although more weakly, in FWCO₂ (Figure 7d). It is
276 not seen in CO₂, and must therefore be driven by the additional freshwater flux. In FWCO₂, the
277 competing effects of the increasing freshwater and CO₂ result in increased sea ice production over
278 the continental shelf in the Ross and Weddell Seas, and also in the Indian Ocean, as shown by the
279 negative (blue) anomaly in Figure 7d. In the western Weddell Sea, there is an area of sea ice melt
280 in PICOntrol, that is reduced FWCO₂, and also in both FW and CO₂, showing that this local effect
281 follows from the increases in CO₂, and from the additional freshwater. The northern sea ice extent
282 in FWCO₂ (Figure 7d) is similar to that in PICOntrol, showing that the increasing Antarctic melt
283 flux has effectively balanced the sea ice retreat induced by the CO₂, in agreement with Figure 5.

284 *Effects on Water Mass Formation*

285 As sea ice forms, brine is rejected, increasing the salinity of the ambient water. Ordinarily, in
286 some places of rapid sea ice production over the continental shelf around Antarctica, this saline
287 water is dense enough to sink to the depth of the shelf, and to spill over the shelf edge and spread

288 through the deep ocean abyss as Antarctic Bottom Water (AABW) (M. van Aken 2007; Nicholls
289 et al. 2009). Another mechanism for AABW formation is prolonged deep convection in the open
290 ocean, which is the primary mechanism by which AABW forms in most CMIP5 climate models
291 but occurs rarely in reality (Heuzé et al. 2015; Cheon and Gordon 2019). Deep water convection
292 does not occur in this configuration of HadGEM3-GC3.1 (Menary et al. 2018). Although the
293 process of bottom water formation has not been definitively determined, a strong salinity driven
294 overturning at the Weddell Sea shelf break has been identified (Menary et al. 2018). The model
295 physics and resolution are similar to ACCESS-OM 1.0, in which AABW is predominantly formed
296 through convection over the continental shelf and subsequent transport of the dense sinking water
297 over the shelf edge (Lago and England 2019). Changes to either the rate (Figure 5), or the locations
298 (Figure 7), of Antarctic sea ice production in our model, may therefore result in changes to the
299 mixed layer depth and to rates of AABW formation.

300 While seawater freezing into sea ice generally results in a deepening of the mixed layer as de-
301 scribed above, melting ice shelves can also drive a deepening of the mixed layer if their melt rate
302 is high enough (Merino et al. 2018; Mackie et al. submitted). This is seen in some places along the
303 coast in FW, where a high volume of buoyant ice shelf basal meltwater enters the ocean at depth
304 and rises to the surface, resulting in a local overturning circulation (Figure 8c). This overturning
305 brings warmer waters to the surface, encouraging the formation and persistence of shore leads,
306 which then promote sea ice production through enhanced frazil ice production, further contribut-
307 ing to persistence of the overturning through the associated brine rejection (Jourdain et al. 2017;
308 Merino et al. 2018). Note that the freezing water in this case is relatively fresh and therefore asso-
309 ciated with relatively weak brine rejection, and so while the surface water becomes saline enough
310 to sustain the overturning (i.e., more saline than the rising freshwater), it is not dense enough to
311 form AABW (density changes are shown in Figure S3 in the online supplemental material and

312 discussed further in Mackie et al. (submitted)). In FWCO₂ (Figure 8d), where ice shelf basal melt
313 rates are equal to those in FW, and enter the ocean with the same vertical and spatial distribution,
314 this increased overturning at the coast is offset by the increasing CO₂, which reduces the temper-
315 ature difference between the ocean surface and the air, and so shallows the mixed layer (Figure
316 8b).

317 In other areas, where the depth or rate of ice shelf basal meltwater entering the ocean is insuf-
318 ficient to initialize a local overturning, the freshwater sits at the surface and forms a cap atop the
319 water column, inhibiting further mixing and shallowing the mixed layer in FW. For example, the
320 blue areas next to the coast in Figure 8c in the eastern Weddell Sea, the western Indian Ocean and
321 parts of the Ross Sea, where the ice shelf melt rates and depths are relatively small (see Rignot
322 et al. (2013), including supplementary materials). In these areas, the surface freshening enhances
323 the shallowing of the mixed layer driven by the increasing CO₂ to result in a strong shallowing in
324 FWCO₂, relative to PICOntrol (Figure 8d).

325 To assess any impact on AABW, we use its northward transport as a proxy for formation rate.
326 To compute the transport, we zonally integrate the meridional velocity at 30° S and then integrate
327 this result vertically from the bottom of the ocean. We define the AABW transport as the first
328 maximum of this function (following Heuzé et al. (2015) and Mackie et al. (submitted)) (Figure
329 9a). The increased meltwater fluxes drive an increase in sea ice production, which may ordinarily
330 be associated with increased AABW formation as described above. However, under pre-industrial
331 conditions in FW, the high volume of ice shelf basal meltwater causes a freshening of the whole
332 water column, and consequently a reduction in AABW formation as water sinking to the shelf
333 is less dense and therefore does not spill off and spread to fill the ocean abyss, (Mackie et al.
334 submitted). In the final 20 years of FW, AABW transport is 2.8 Sv weaker than in PICOntrol
335 (Table 3). As CO₂ increases in CO₂, the warming of the ocean makes the waters less dense, and

336 so also drives a decrease in AABW formation. This results in AABW transport in the final 20
337 years of CO₂ being 3.9 Sv weaker than in PIControl. The effect of increasing both ice shelf melt
338 and CO₂ in FWCO₂ is a slightly stronger decrease in AABW formation than in either FW or CO₂,
339 since in FWCO₂ both the warming and the freshening drivers are present, and AABW transport for
340 the final 20 years of FWCO₂ is 4.6 Sv weaker than in PIControl. The changes in density that drive
341 these changes in AABW transport are very small (of the order 0.01 kgm⁻³), and are plotted in the
342 online supplemental material (Figure S3). A student t-test for related samples, comparing AABW
343 for the final 20 years of each of the experiments with that in PIControl for the same period, shows
344 all these changes to be statistically significant at a greater than 99% confidence level (Table 3).
345 Although the mechanism for the decline in AABW formation in FWCO₂ is partly a freshening of
346 the whole water column, rather than increased stratification as found by Lago and England (2019),
347 these findings do support the suggestion raised in that work that the decline in AABW formation
348 projected under global warming scenarios may be weaker than in reality if the projections do not
349 account for increasing melt fluxes from Antarctica.

350 Changes in AABW export from the Antarctic have been linked to changes in the Atlantic Merid-
351 ional Overturning Circulation (AMOC) (Weaver et al. 2003; Swingedouw et al. 2009), which is
352 important to Northern Hemisphere climate (Buckley and Marshall 2016; Sévellec and Fedorov
353 2016). A reduction in AABW export can allow the AMOC to reach further south in the Atlantic at
354 greater depth (Swingedouw et al. 2009). We therefore examine both the strength (Figure 9b) and
355 depth (Figure 9c) of the AMOC at 30° S. We integrate the meridional velocity at 30° S through the
356 Atlantic basin from coast to coast. We then integrate this result over depth, from the bottom of the
357 ocean to the surface. We define the AMOC strength at 30° S as the maximum of this integrated
358 transport in the southward direction (following Heuzé et al. (2015)), and the AMOC depth as the
359 depth at which this maximum occurs. We use a student t-test to compare the AMOC strength

360 and depth for final 20 years of the experiments with that in PIControl for the same period, and
361 assess the significance of any change (Table 3). In PIControl, the mean AMOC strength is 14.22
362 Sv. In FW, there is a small strengthening (0.4 Sv), significant at the 95 % confidence level, and
363 the AMOC becomes slightly deeper (by 32 m) at 30° S in response to the reduced AABW trans-
364 port, (Figure 9c). In CO₂, the AMOC weakens by 2.5 Sv and becomes around 108 m shallower
365 (relative to PIControl), following the CO₂-induced warming (see also Rahmstorf et al. (2015))
366 (Figure 9b, c). The CO₂-induced weakening and shallowing of the AMOC in CO₂ are greater
367 than the changes driven by the reduced AABW transport following the increased ice shelf melt
368 in FW, and are statistically more significant with a confidence level exceeding 99 %. In FWCO₂,
369 the CO₂-induced weakening and shallowing of the AMOC may be slightly offset by the effects of
370 the reduced AABW transport in the second half of the simulations (when the reduction in AABW
371 transport is greater in FWCO₂ than in CO₂ (Figure 9a)), although the variability of the AMOC
372 in all the simulations means a longer timeseries would be required to conclude this definitively
373 (Figure 9b). This suggests that, while climate projections that neglect increasing Antarctic melt
374 fluxes may underestimate the future decline in AABW, they may slightly overestimate the decline
375 in the AMOC at southern latitudes.

376 *Surface Ocean Effects*

377 An increasing volume of meltwater entering the Southern Ocean causes surface waters to cool
378 and freshen, as buoyant fresh water sits at the surface and drives stratification of the water column,
379 and these effects may extend into the Northern Hemisphere (Richardson et al. 2005; Pauling et al.
380 2017; Bronselaer et al. 2018; Mackie et al. submitted). Globally increasing CO₂ causes the ocean
381 to warm everywhere, and we consider whether the effect of a simultaneous increase in meltwater
382 could partially offset this (Figure 10). Similar effects were found for all seasons (not shown).

383 The strong warming that occurs everywhere in CO₂, as a result of the increasing CO₂, is reduced
384 slightly in the tropical Pacific, the North Atlantic, and in the north-western Indian Ocean as a result
385 of the increased Antarctic mass loss in FWCO₂, but the warming in these areas is not reversed.
386 A stronger reduction in the surface warming occurs in the southern Indian, Atlantic and Pacific
387 Oceans, closer to the source of the melt perturbation. Closer to Antarctica, in the outer Ross Sea
388 and in the southern Western Pacific, the warming in CO₂ is replaced by a cooling in FWCO₂
389 (relative to PControl), while waters next to the coast are likely to be at, or close to, their freezing
390 temperature in all simulations, and therefore do not cool further. The increasing melt volume
391 in FWCO₂ does not significantly alter the changes in surface salinity seen in CO₂ (which are
392 attributable to increasing CO₂), except at very high southern latitudes, where there is increased
393 freshening (shown in the online supplementary material (Figure S4)).

394 Under pre-industrial conditions in FW, surface cooling and freshening from the increased ice
395 shelf melt flux causes an increase in near surface ocean density at high southern latitudes that is
396 mainly temperature-driven (see Mackie et al. (submitted) for more details of this effect). This
397 reduces the meridional density gradient across the Southern Ocean, driving a reduction in the
398 Antarctic Circumpolar Current (ACC) volume transport, potentially altering the flow of heat to the
399 high latitude ocean (Russell et al. 2006; Mackie et al. submitted). The response of the ACC to the
400 increasing melt in FWCO₂ is similar to that in FW for the first 50 years, however as both CO₂ and
401 the melt increase further over the final 50 years, the ACC transport in FWCO₂ becomes similar
402 to that in CO₂, where only CO₂ is increasing. This is because the CO₂-induced warming of the
403 surface ocean in FWCO₂ greatly reduces the near-surface density everywhere (a plot of the density
404 anomalies is included in Figure S3 in the online supplemental material). The additional melt in
405 FWCO₂ drives a surface cooling at high latitudes, but after 50 years, this is weaker than in FW
406 (Figure 10), and the density changes resulting from the additional melt in FWCO₂ are therefore

407 not strong enough to alter the meridional density gradient and impact the ACC in the second half
408 of the simulation (Figure 11).

409 *Effects on Wind Stress*

410 The westerly wind belt around Antarctica is driven in part by the meridional gradient in the
411 vertical exchange of heat between the ocean and atmosphere (Kidston et al. 2011). Sea ice insu-
412 lates the ocean surface and so inhibits this flux at high latitudes, suggesting a link between sea
413 ice extent and the strength and position of the winds that has been investigated in several studies
414 (Menéndez et al. 1999; Kidston et al. 2011; Bader et al. 2013; Grise and Polvani 2016; Bracegir-
415 dle et al. 2018). Surface cooling also reduces the ocean to atmosphere heat flux, strengthening the
416 westerly winds (Mackie et al. submitted). Increasing meltwater offsets the CO₂-induced decline
417 in sea ice extent (Figure 6) and cools the ocean surface (Figure 10), and so we consider whether
418 the strengthening of the winds that is generally associated with increasing CO₂ (Swart and Fyfe
419 2012) may be affected by the increased meltwater.

420 The sensitivity of the surface wind stress to sea ice concentration is greatest in August September
421 and October (Kidston et al. 2011) at maximum sea ice extent. The simulated zonal mean westerly
422 wind stress, at this time, is shown in Figure 12. Both the increased CO₂ (CO2) and the increased
423 melt fluxes (FW) drive an increase in wind stress at the surface, which we interpret as an increase
424 in jet strength. The greatest strengthening of the wind stress occurs when both forcings are applied
425 together in FWCO2 (Figure 12). To assess whether there was a significant change by the end of
426 the experiments, the mean strength and position for the peak wind stress over the final 20 years
427 of each experiment were compared to those for PIControl, averaged over the same period, using
428 a t-test for related samples to calculate the significance. We calculated the strength and position
429 of the peak wind stress from a quadratic curve fitted to the three model grid points surrounding

430 the maximum wind stress (Figure 12) for the comparison (Table 2). There is no significant change
431 to the latitude for the maximum wind stress in any of the experiments. Increasing the meltwater
432 fluxes in FW results in the peak wind stress increasing by 0.019 Nm^{-2} at the 95% confidence level,
433 and the increasing CO_2 in CO_2 drives an increase of 0.033 Nm^{-2} at a confidence level greater than
434 99%. The greatest increase in strength, 0.043 Nm^{-2} , is in FW CO_2 , when both drivers are present.
435 Including increasing Antarctic meltwater fluxes may therefore partially address the bias common
436 to many climate models, whereby the simulated westerly winds are too weak when compared to
437 reanalysis data (Bracegirdle et al. 2013).

438 **4. Summary**

439 Almost all the projections in CMIP5 and CMIP6 suggest a strong decline in Antarctic sea ice
440 under future climate warming scenarios, but none of these models include an increase in the ice
441 shelf melt fluxes from Antarctica. Our results show that these increasing melt fluxes may enhance
442 sea ice growth and partially offset a CO_2 -induced decline in Antarctic sea ice area and thickness.

443 We have shown that including increasing ice sheet melt fluxes in climate models could reduce
444 some model biases, and our results demonstrate the importance of considering the effect of com-
445 bined forcings when determining sensitivities for future climate projections. Some responses to
446 increasing ice shelf melt fluxes in the Southern Ocean may be balanced by increasing levels of
447 CO_2 . For example, the local overturning of Antarctic coastal waters, initiated by large increases in
448 ice shelf basal melt entering the ocean at depth, is inhibited if CO_2 increases simultaneously with
449 the melt rate. The separate forcings (increasing CO_2 and increasing Antarctic mass loss) combine
450 to result in a greater reduction in AABW formation and a greater strengthening of westerly wind
451 stress than is seen when either forcing is applied in isolation. In other areas, the warming effect of
452 the CO_2 is partially countered by the increasing melt flux. For example, slightly more moderate

453 surface temperature increases are seen in the Southern Ocean and there is no clear net reduction
454 in sea ice area. The reduction in the ACC that follows from density changes induced by increased
455 ice shelf basal melt, is not seen when CO₂ increases simultaneously, because of the more severe
456 and widespread density changes associated with the CO₂ increase.

457 These are idealised experiments and the increase implemented for the Antarctic melt rate was
458 spatially uniform, whereas in reality it is likely that melt rates will accelerate more for some ice
459 shelves than for others, which may alter the sensitivities found here. Similarly, the increase in CO₂
460 is also idealised and the impact of increasing CO₂, and the sensitivity of this to increasing melt
461 rates, will depend on future emission rates for greenhouse gases.

462 Increasing Antarctic melt fluxes, which are more likely as the ocean warms and ice shelves
463 become negatively mass-balanced, have an impact on global climate. Future climate projections
464 that neglect the increasing melt rates are likely to over-estimate both Antarctic sea ice decline and
465 some ocean surface warming in the Southern Hemisphere. Similarly, both the decrease in AABW
466 formation, and the strengthening of the westerly winds around Antarctica may be under-estimated
467 in current climate projections. The effects of increasing CO₂ and increasing melt fluxes are inter-
468 active and their combined effect is not a linear sum of the effects that they drive individually (i.e.,
469 when implemented separately). It is therefore important that increasing Antarctic melt fluxes be
470 realistically represented in climate models, perhaps through an embedded dynamic ice sheet model,
471 in order that the impact of future warming on sea ice, ocean and climate be reliably projected.

472 *Acknowledgments.* This project was funded by the New Zealand Deep South National Science
473 Challenge, MBIE contract C01X142. Data for PIControl and CO₂ were calculated by the Hadley
474 Centre, U.K. Met Office for submission to the CMIP6 experiment. The project is grateful for
475 support from Professor Bitz at University of Washington. We acknowledge use of the Monsoon2

476 system, and the High Capacity Central File Storage Service at University of Otago, New Zealand.
477 Model data analysed in this work are publicly available at Mackie et al. (2020).

478 **References**

479 Andreas, E. L., and B. Murphy, 1986: Bulk transfer coefficients for heat and momentum over
480 leads and polynyas. *Journal of Physical Oceanography*, **16 (11)**, 1875–1883, doi:10.1175/
481 1520-0485(1986)016<1875:BTCFHA>2.0.CO;2.

482 Bader, J., M. Flügge, N. G. Kvamstø, M. D. S. Mesquita, and A. Voigt, 2013: Atmospheric
483 winter response to a projected future Antarctic sea-ice reduction: a dynamical analysis. *Climate*
484 *Dynamics*, **40 (11)**, 2707–2718, doi:10.1007/s00382-012-1507-9.

485 Bigg, G. R., M. R. Wadley, D. P. Stevens, and J. A. Johnson, 1997: Modelling the dynamics
486 and thermodynamics of icebergs. *Cold Regions Science and Technology*, **26 (2)**, 113 – 135,
487 doi:https://doi.org/10.1016/S0165-232X(97)00012-8.

488 Bintanja, R., G. van Oldenborgh, and C. Katsman, 2015: The effect of increased fresh water
489 from Antarctic ice shelves on future trends in Antarctic sea ice. *Annals of Glaciology*, **56 (69)**,
490 120126, doi:10.3189/2015AoG69A001.

491 Bintanja, R., G. J. van Oldenborgh, S. S. Drijfhout, B. Wouters, and C. A. Katsman, 2013: Impor-
492 tant role for ocean warming and increased ice-shelf melt in Antarctic sea-ice expansion. *Nature*
493 *Geoscience*, **6**, 376 EP –.

494 Bracegirdle, T. J., P. Hyder, and C. R. Holmes, 2018: CMIP5 diversity in southern westerly jet
495 projections related to historical sea ice area: Strong link to strengthening and weak link to shift.
496 *Journal of Climate*, **31 (1)**, 195–211, doi:10.1175/JCLI-D-17-0320.1.

- 497 Bracegirdle, T. J., E. Shuckburgh, J.-B. Sallee, Z. Wang, A. J. S. Meijers, N. Bruneau, T. Phillips,
498 and L. J. Wilcox, 2013: Assessment of surface winds over the Atlantic, Indian, and Pacific
499 Ocean sectors of the Southern Ocean in CMIP5 models: historical bias, forcing response, and
500 state dependence. *Journal of Geophysical Research: Atmospheres*, **118** (2), 547–562, doi:10.
501 1002/jgrd.50153.
- 502 Bromwich, D. H., B. Chen, K. M. Hines, and R. I. Cullather, 1998: Global atmospheric responses
503 to Antarctic forcing. *Annals of Glaciology*, **27**, 521–527, doi:10.3189/1998AoG27-1-521-527.
- 504 Bronselaer, B., M. Winton, S. M. Griffies, W. J. Hurlin, K. B. Rodgers, O. V. Sergienko, R. J.
505 Stouffer, and J. L. Russell, 2018: Change in future climate due to Antarctic meltwater. *Nature*,
506 doi:10.1038/s41586-018-0712-z.
- 507 Buckley, M. W., and J. Marshall, 2016: Observations, inferences, and mechanisms of the Atlantic
508 meridional overturning circulation: A review. *Reviews of Geophysics*, **54** (1), 5–63, doi:10.1002/
509 2015RG000493.
- 510 Cavalieri, D. J., and C. L. Parkinson, 2008: Antarctic sea ice variability and trends, 1979–2006.
511 *Journal of Geophysical Research: Oceans*, **113** (C7), doi:10.1029/2007JC004564.
- 512 Cheon, W. G., and A. L. Gordon, 2019: Open-ocean polynyas and deep convection in the Southern
513 Ocean. *Scientific Reports*, **9** (1), 6935, doi:10.1038/s41598-019-43466-2.
- 514 Dai, M., H. H. Shen, M. A. Hopkins, and S. F. Ackley, 2004: Wave rafting and the equilibrium
515 pancake ice cover thickness. *Journal of Geophysical Research: Oceans*, **109** (C7), doi:10.1029/
516 2003JC002192.
- 517 DeConto, R. M., and D. Pollard, 2016: Contribution of Antarctica to past and future sea-level rise.
518 *Nature*, **531**, 591 EP –, article.

- 519 Grise, K. M., and L. M. Polvani, 2016: Is climate sensitivity related to dynamical sensitivity? *Journal of Geophysical Research: Atmospheres*, **121** (10), 5159–5176, doi:10.1002/2015JD024687.
- 520
- 521 Heuzé, C., K. J. Heywood, D. P. Stevens, and J. K. Ridley, 2015: Changes in global ocean bottom
522 properties and volume transports in CMIP5 models under climate change scenarios. *Journal of*
523 *Climate*, **28** (8), 2917–2944, doi:10.1175/JCLI-D-14-00381.1.
- 524 Hoskins, B. J., and K. I. Hodges, 2005: A new perspective on southern hemisphere storm tracks.
525 *Journal of Climate*, **18** (20), 4108–4129, doi:10.1175/JCLI3570.1.
- 526 Jourdain, N. C., P. Mathiot, N. Merino, G. Durand, J. Le Sommer, P. Spence, P. Dutrieux, and
527 G. Madec, 2017: Ocean circulation and sea-ice thinning induced by melting ice shelves in the
528 Amundsen Sea. *Journal of Geophysical Research: Oceans*, **122** (3), 2550–2573, doi:10.1002/
529 2016JC012509, URL <https://agupubs.onlinelibrary.wiley.com/doi/abs/10.1002/2016JC012509>,
530 <https://agupubs.onlinelibrary.wiley.com/doi/pdf/10.1002/2016JC012509>.
- 531 Kidston, J., A. S. Taschetto, D. W. J. Thompson, and M. H. England, 2011: The influence of
532 southern hemisphere sea-ice extent on the latitude of the mid-latitude jet stream. *Geophysical*
533 *Research Letters*, **38** (15), doi:10.1029/2011GL048056.
- 534 Kuhlbrodt, T., and Coauthors, 2018: The lowresolution version of HadGEM3 GC3.1: Devel-
535 opment and evaluation for global climate. *Journal of Advances in Modeling Earth Systems*,
536 doi:10.1029/2018MS001370.
- 537 Lago, V., and M. H. England, 2019: Projected slowdown of Antarctic Bottom Water formation
538 in response to amplified meltwater contributions. *Journal of Climate*, **32** (19), 6319–6335, doi:
539 10.1175/JCLI-D-18-0622.1.

- 540 Le Quéré, C., and Coauthors, 2007: Saturation of the Southern Ocean CO₂ sink due to recent
541 climate change. *Science*, **316 (5832)**, 1735–1738, doi:10.1126/science.1136188.
- 542 Liston, G. E., and J.-G. Winther, 2005: Antarctic surface and subsurface snow and ice melt fluxes.
543 *Journal of Climate*, **18 (10)**, 1469–1481, doi:10.1175/JCLI3344.1.
- 544 M. van Aken, H., 2007: *The Oceanic Thermohaline Circulation: An Introduction*, Atmo-
545 spheric and Oceanographic Sciences Library, Vol. 39. Springer-Verlag, New York, doi:10.1007/
546 978-0-387-48039-8.
- 547 Mackie, S., I. J. Smith, J. K. Ridley, D. P. Stevens, and P. J. Langhorne, 2020: Climate model
548 response to increasing Antarctic iceberg and ice shelf melt. PANGAEA, URL [https://doi.org/](https://doi.org/10.1594/PANGAEA.911392)
549 [10.1594/PANGAEA.911392](https://doi.org/10.1594/PANGAEA.911392), doi:10.1594/PANGAEA.911392.
- 550 Mackie, S., I. J. Smith, J. K. Ridley, D. P. Stevens, and P. J. Langhorne, submitted: Climate
551 response to increasing Antarctic iceberg and ice shelf melt. *Journal of Climate*, **this issue**.
- 552 Maksym, T., 2012: Antarctic sea ice a polar opposite? *Oceanography*, URL [https://doi.org/10.](https://doi.org/10.5670/oceanog.2012.88)
553 [5670/oceanog.2012.88](https://doi.org/10.5670/oceanog.2012.88).
- 554 Marsh, R., and Coauthors, 2015: NEMO-ICB (v1.0): interactive icebergs in the NEMO ocean
555 model globally configured at eddy-permitting resolution. *Geoscientific Model Development*,
556 **8 (5)**, 1547–1562, doi:10.5194/gmd-8-1547-2015.
- 557 Marsland, S. J., J. A. Church, N. L. Bindoff, and G. D. Williams, 2007: Antarctic coastal polynya
558 response to climate change. *Journal of Geophysical Research: Oceans*, **112 (C7)**, doi:10.1029/
559 [2005JC003291](https://doi.org/10.1029/2005JC003291).

- 560 Martin-Espanol, A., and Coauthors, 2016: Spatial and temporal Antarctic Ice Sheet mass trends,
561 glacio-isostatic adjustment, and surface processes from a joint inversion of satellite altimeter,
562 gravity, and GPS data. *Journal of Geophysical Research: Earth Surface*, **121** (2), 182–200.
- 563 Mathiot, P., A. Jenkins, C. Harris, and G. Madec, 2017: Explicit representation and parametrised
564 impacts of under ice shelf seas in the z^* coordinate ocean model NEMO 3.6. *Geoscientific Model*
565 *Development*, **10** (7), 2849–2874, doi:10.5194/gmd-10-2849-2017.
- 566 Menary, M. B., and Coauthors, 2018: Preindustrial control simulations with HadGEM3-GC3.1
567 for CMIP6. *Journal of Advances in Modeling Earth Systems*, **10** (12), 3049–3075, doi:10.1029/
568 2018MS001495.
- 569 Menéndez, C. G., V. Serafini, and H. Le Treut, 1999: The effect of sea-ice on the transient
570 atmospheric eddies of the southern hemisphere. *Climate Dynamics*, **15** (9), 659–671, doi:
571 10.1007/s003820050308.
- 572 Merino, N., N. C. Jourdain, J. L. Sommer, H. Goosse, P. Mathiot, and G. Durand, 2018: Impact of
573 increasing Antarctic glacial freshwater release on regional sea-ice cover in the Southern Ocean.
574 *Ocean Modelling*, **121**, 76 – 89, doi:https://doi.org/10.1016/j.ocemod.2017.11.009.
- 575 Nicholls, K. W., S. sterhus, K. Makinson, T. Gammelsrd, and E. Fahrbach, 2009: Ice-ocean pro-
576 cesses over the continental shelf of the southern Weddell Sea, Antarctica: A review. *Reviews of*
577 *Geophysics*, **47** (3), doi:10.1029/2007RG000250.
- 578 Pauling, A. G., C. M. Bitz, I. J. Smith, and P. J. Langhorne, 2016: The response of the Southern
579 Ocean and Antarctic sea ice to freshwater from ice shelves in an Earth System Model. *Journal*
580 *of Climate*, 1655–1672.

- 581 Pauling, A. G., I. J. Smith, P. J. Langhorne, and C. M. Bitz, 2017: Time-dependent freshwater
582 input from ice shelves: Impacts on Antarctic sea ice and the Southern Ocean in an Earth System
583 Model. *Geophysical Research Letters*, **44** (20), 10,454–10,461, doi:10.1002/2017GL075017.
- 584 Rahmstorf, S., J. E. Box, G. Feulner, M. E. Mann, A. Robinson, S. Rutherford, and E. J. Schaffer-
585 nicht, 2015: Exceptional twentieth-century slowdown in Atlantic Ocean overturning circulation.
586 *Nature Climate Change*, **5**, 475 EP –, article.
- 587 Richardson, G., M. R. Wadley, K. J. Heywood, D. P. Stevens, and H. T. Banks, 2005: Short-term
588 climate response to a freshwater pulse in the Southern Ocean. *Geophysical Research Letters*,
589 **32** (3), doi:10.1029/2004GL021586.
- 590 Ridley, J. K., E. W. Blockley, A. B. Keen, J. G. L. Rae, A. E. West, and D. Schroeder, 2018:
591 The sea ice model component of HadGEM3-GC3.1. *Geoscientific Model Development*, **11** (2),
592 713–723, doi:10.5194/gmd-11-713-2018.
- 593 Rignot, E., J. L. Bamber, M. R. van den Broeke, C. Davis, Y. Li, W. J. van de Berg, and E. van
594 Meijgaard, 2008: Recent Antarctic ice mass loss from radar interferometry and regional climate
595 modelling. *Nature Geoscience*, **1**, 106 EP –.
- 596 Rignot, E., S. Jacobs, J. Mouginot, and B. Scheuchl, 2013: Ice-shelf melting around Antarctica.
597 *Science*, **341** (6143), 266–270, doi:10.1126/science.1235798.
- 598 Rind, R., R. Healy, C. Parkinson, and D. Martinson, 1995: The role of sea ice in 2xCO₂ climate
599 model sensitivity. Part I: The total influence of sea ice thickness and extent. *Journal of Climate*
600 - *J CLIMATE*, **8**, 449–463, doi:10.1175/1520-0442(1995)008<0449:TROSII>2.0.CO;2.

601 Russell, J. L., R. J. Stouffer, and K. W. Dixon, 2006: Intercomparison of the Southern Ocean
602 circulations in IPCC coupled model control simulations. *Journal of Climate*, **19** (18), 4560–
603 4575, doi:10.1175/JCLI3869.1.

604 Sévellec, F., and A. V. Fedorov, 2016: AMOC sensitivity to surface buoyancy fluxes: Stronger
605 ocean meridional heat transport with a weaker volume transport? *Climate Dynamics*, **47** (5),
606 1497–1513, doi:10.1007/s00382-015-2915-4.

607 Shepherd, A., and Coauthors, 2018: Mass balance of the Antarctic Ice Sheet from 1992 to 2017.
608 *Nature*, **558** (7709), 219–222, doi:10.1038/s41586-018-0179-y.

609 Sloyan, B. M., 2006: Antarctic bottom and lower circumpolar deep water circulation in the
610 eastern Indian Ocean. *Journal of Geophysical Research: Oceans*, **111** (C2), doi:10.1029/
611 2005JC003011.

612 Smedsrud, L. H., and R. Skogseth, 2006: Field measurements of arctic grease ice properties and
613 processes. *Cold Regions Science and Technology*, **44**, 171–183, doi:10.1016/j.coldregions.2005.
614 11.002.

615 Stammerjohn, S. E., D. G. Martinson, R. C. Smith, X. Yuan, and D. Rind, 2008: Trends in
616 Antarctic annual sea ice retreat and advance and their relation to El Niño Southern Oscillation
617 and Southern Annular Mode variability. *Journal of Geophysical Research: Oceans*, **113** (C3),
618 doi:10.1029/2007JC004269.

619 Storkey, D., and Coauthors, 2018: UK Global Ocean GO6 and GO7: a traceable hierarchy
620 of model resolutions. *Geoscientific Model Development*, **11** (8), 3187–3213, doi:10.5194/
621 gmd-11-3187-2018.

- 622 Sutterley, T. C., I. Velicogna, E. Rignot, J. Mouginot, T. Flament, M. R. Van Den Broeke, J. M.
623 Van Wessem, and C. H. Reijmer, 2014: Mass loss of the Amundsen Sea Embayment of West
624 Antarctica from four independent techniques. *Geophysical Research Letters*, **41** (23), 8421–
625 8428.
- 626 Swart, N. C., and J. C. Fyfe, 2012: Observed and simulated changes in the southern hemisphere
627 surface westerly wind-stress. *Geophysical Research Letters*, **39** (L16711), 1–6, doi:10.1029/
628 2012GL052810.
- 629 Swart, N. C., and J. C. Fyfe, 2013: The influence of recent Antarctic ice sheet retreat on simulated
630 sea ice area trends. *Geophysical Research Letters*, **40**, 4328–4332.
- 631 Swingedouw, D., T. Fichefet, H. Goosse, and M. F. Loutre, 2009: Impact of transient freshwater
632 releases in the Southern Ocean on the AMOC and climate. *Climate Dynamics*, **33** (2-3), 365–
633 381.
- 634 Timmermann, R., and H. H. Hellmer, 2013: Southern Ocean warming and increased ice shelf
635 basal melting in the twenty-first and twenty-second centuries based on coupled ice-ocean finite-
636 element modelling. *Ocean Dynamics*, **63** (9), 1011–1026, doi:10.1007/s10236-013-0642-0.
- 637 Turner, J., T. J. Bracegirdle, T. Phillips, G. J. Marshall, and J. S. Hosking, 2013: An initial assess-
638 ment of Antarctic sea ice extent in the CMIP5 models. *Journal of Climate*, **26** (5), 1473–1484,
639 doi:10.1175/JCLI-D-12-00068.1.
- 640 Turner, J., and Coauthors, 2009: Non-annular atmospheric circulation change induced by
641 stratospheric ozone depletion and its role in the recent increase of Antarctic sea ice ex-
642 tent. *Geophysical Research Letters*, **36** (8), doi:10.1029/2009GL037524, URL <https://agupubs>.

643 onlinelibrary.wiley.com/doi/abs/10.1029/2009GL037524, <https://agupubs.onlinelibrary.wiley.com/doi/pdf/10.1029/2009GL037524>.

644

645 Walters, D., and Coauthors, 2019: The Met Office Unified Model Global Atmosphere 7.0/7.1 and
646 JULES Global Land 7.0 configurations. *Geoscientific Model Development*, **12** (5), 1909–1963,
647 doi:10.5194/gmd-12-1909-2019.

648 Weaver, A. J., O. A. Saenko, P. U. Clark, and J. X. Mitrovica, 2003: Meltwater Pulse 1A from
649 Antarctica as a trigger of the Bølling-Allerød Warm Interval. *Science*, **299** (5613), 1709–1713,
650 doi:10.1126/science.1081002.

651 Weeks, W., 2010: *On Sea Ice*. University of Alaska Press, URL <https://books.google.co.nz/books?id=9S55O6WzuL8C>.

652

653 Williams, J., and Coauthors, 2016: Development of the New Zealand Earth System Model:
654 NZESM. *Weather and Climate*, **36**, 25–44.

655 Williams, K. D., and Coauthors, 2017: The Met Office Global Coupled Model 3.0 and 3.1 (GC3.0
656 and GC3.1) configurations. *Journal of Advances in Modeling Earth Systems*, **10** (2), 357–380,
657 doi:10.1002/2017MS001115.

658 Winsor, P., and G. Björk, 2000: Polynya activity in the Arctic Ocean from 1958 to 1997. *Journal
659 of Geophysical Research: Oceans*, **105** (C4), 8789–8803, doi:10.1029/1999JC900305.

660 Yuan, N., M. Ding, J. Ludescher, and A. Bunde, 2017: Increase of the Antarctic sea ice extent is
661 highly significant only in the Ross Sea. *Scientific Reports*, **7**, 41 096, article.

662 Zunz, V., and H. Goosse, 2015: Influence of freshwater input on the skill of decadal forecast of
663 sea ice in the Southern Ocean. *The Cryosphere*, **9** (2), 541–556, doi:10.5194/tc-9-541-2015.

664 **LIST OF TABLES**

665 **Table 1.** Summary of experiment and control simulation settings. 32

666 **Table 2.** Difference between the mean peak westerly wind stress over the Southern
667 Ocean for each experiment and PControl for the final 20 years of the simu-
668 lations. The peak strength is the strength at the peak location in Figure 12,
669 determined as described in the text. The significance of any change is given by
670 the p-value (following from calculation of the t-score for related samples). A
671 p-value of less than 0.05 indicates significance at the 95% confidence level. 33

672 **Table 3.** Difference in the mean AABW and AMOC transport and AMOC depth be-
673 tween each experiment and PControl for the final 20 years of the simulations.
674 The significance of any change is given by the p-value (following from calcu-
675 lation of the t-score for related samples). A p-value of less than 0.05 indicates
676 significance at the 95% confidence level. 34

TABLE 1. Summary of experiment and control simulation settings.

Model Simulation	Other External Forcings	Increasing Mass Loss
PIControl	Fixed Pre-Industrial	N
FW	Fixed Pre-Industrial	Y
CO2	CO ₂ increasing by 1% per year	N
FWCO2	CO ₂ increasing by 1% per year	Y

677 TABLE 2. Difference between the mean peak westerly wind stress over the Southern Ocean for each exper-
678 iment and PControl for the final 20 years of the simulations. The peak strength is the strength at the peak
679 location in Figure 12, determined as described in the text. The significance of any change is given by the p-value
680 (following from calculation of the t-score for related samples). A p-value of less than 0.05 indicates significance
681 at the 95% confidence level.

Simulation	Δ Latitude ($^{\circ}$)	p-value	Δ Strength (Nm^{-2})	p-value
CO2	-0.687	0.646	0.033	2.49E-07
FW	-1.045	0.379	0.019	0.011
FWCO2	-1.107	0.428	0.043	2.59E-08

682 TABLE 3. Difference in the mean AABW and AMOC transport and AMOC depth between each experiment
 683 and PControl for the final 20 years of the simulations. The significance of any change is given by the p-value
 684 (following from calculation of the t-score for related samples). A p-value of less than 0.05 indicates significance
 685 at the 95% confidence level.

Simulation	Δ AABW transport (Sv)	p-value	Δ AMOC transport (Sv)	p-value	Δ AMOC Depth (m)	p-value
PControl - CO2	3.914	2.4e-45	2.504	6.0e-31	-107.589	8.9e-64
PControl - FW	2.796	8.3e-30	-0.427	0.014	32.021	1.0e-15
PControl - FWCO2	4.561	7.3e-52	2.145	9.5e-26	-91.720	6.3e-56

686 **LIST OF FIGURES**

687 **Fig. 1.** The total rate of meteoric ice mass loss from the Antarctic continent used for FW and
688 FWCO2. 37

689 **Fig. 2.** (a) Mean spatial distribution of the total melt flux for PICOntrol. (b)-(d) The mean anomaly,
690 with respect to PICOntrol, for the final 20 years of: (b) CO2, (c) FW, and (d) FWCO2.
691 Colour scales for (a), (c) and (d) are logarithmic. Note the different colour scale for the CO2
692 anomaly, where the total volume of meltwater is the same as for PICOntrol, and differences in
693 the spatial distribution follow from the different ocean surface properties in a pre-industrial
694 environment and an environment of increasing CO₂. 38

695 **Fig. 3.** (a) Bathymetry, with the ocean sectors (Ross Sea, Amundsen-Bellinghausen Sea, Weddell
696 Sea, Indian Ocean and Western Pacific) used for discussion of sea ice effects overlaid; (b)
697 Model sea surface height from PICOntrol, with closed contours indicating the centres for the
698 Ross and Weddell Gyres referred to in the text. Note that the flow direction is clockwise for
699 the gyres, and the Antarctic Coastal Current flows anti-clockwise around the continent. 39

700 **Fig. 4.** Total melt flux in each simulation for: (a) whole Southern Hemisphere; (b) Ross Sea; (c)
701 Amundsen-Bellinghausen Sea; (d) Weddell Sea; (e) Indian Ocean; (f) Western Pacific. 40

702 **Fig. 5.** Evolution of sea ice area (SIA) in each simulation for: (a) whole Southern Hemisphere; (b)
703 Ross Sea; (c) Amundsen-Bellinghausen Sea; (d) Weddell Sea; (e) Indian Ocean; (f) Western
704 Pacific (5 year running mean). 41

705 **Fig. 6.** (a) Mean September sea ice thickness (SIT) in PICOntrol. (b)-(d) SIT anomaly for the final
706 30 years of: (b) CO2, (c) FW, and (d) FWCO2. The black contour (white in (a)) shows the
707 mean September sea ice extent (the area beyond which the sea ice concentration in a grid
708 cell does not exceed 15%) for (a) PICOntrol, (b) CO2, (c) FW, and (d) FWCO2. 42

709 **Fig. 7.** (a) The mean downward salt flux for June, July and August in PICOntrol. (b)-(d) Mean
710 anomaly for June, July and August for the final 30 years of: (b) CO2, (c) FW, and (d)
711 FWCO2. See text for an explanation of how this flux can be used as a proxy for sea ice pro-
712 duction and decay. The contours on all panels show the extent of areas of sea ice produc-
713 tion and melt in PICOntrol. 43

714 **Fig. 8.** (a) The mean mixed layer depth for June, July and August in PICOntrol. (b)-(d) Mean
715 anomaly for June, July and August for the final 30 years of: (b) CO2, (c) FW, and (d)
716 FWCO2. Mixed layer depth is defined as the depth at which the potential density of seawater
717 differs from that at 10 m depth by more than 0.01 kgm⁻³. 44

718 **Fig. 9.** (a) The zonal mean maximum AABW transport at 30° S. (b) AMOC strength at 30° S.
719 (c) AMOC depth at 30° S. The 5 year running mean is shown for (a)-(c). See text for a
720 description of calculations for the AMOC strength and depth. 45

721 **Fig. 10.** (a) Mean sea surface temperature (SST) in PICOntrol. (b)-(d) SST anomaly, averaged over
722 the final 30 years of: (b) CO2, (c) FW, and (d) FWCO2. Stippling marks anomalies not
723 significant at the 95% confidence level (using a student's t-test for related samples). 46

724 **Fig. 11.** Annual mean of the Antarctic Circumpolar Current (ACC) transport, calculated as integrated
725 mass transport across the Drake Passage. 47

726 **Fig. 12.** Zonal mean westerly wind stress for August to October, averaged over the final 30 years of
727 the experiments. 48

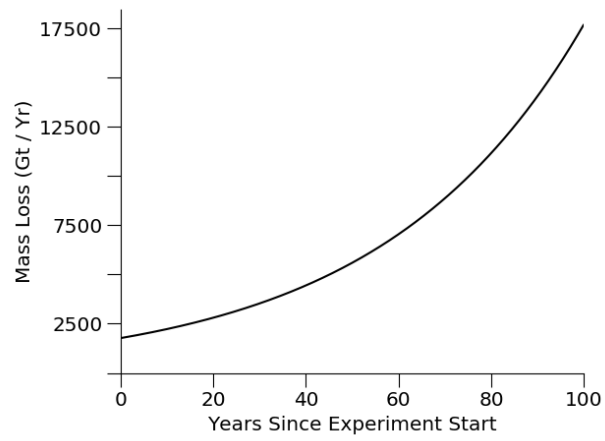


FIG. 1. The total rate of meteoric ice mass loss from the Antarctic continent used for FW and FWCO2.